Simplified Spatial Correlation Models for Clustered MIMO Channels with Different Array Configurations

Antonio Forenza[§], David J. Love[†], and Robert W. Heath Jr.[‡].

[§]Rearden, LLC
355 Bryant Street, Suite 110
San Francisco, CA 94107 USA
antonio@rearden.com

[†]School of Electrical and Computer Engineering
Purdue University
EE Building
465 Northwestern Ave.
West Lafayette, IN 47907 USA
djlove@ecn.purdue.edu

[‡]Wireless Networking and Communications Group
Department of Electrical and Computer Engineering
The University of Texas at Austin
1 University Station C0803
Austin, TX 78712-0240 USA
Phone: +1-512-425-1305
Fax: +1-512-471-6512
rheath@ece.utexas.edu

Abstract

An approximate spatial correlation model for clustered MIMO channels is proposed in this paper. The two ingredients for the model are an approximation for uniform linear and circular arrays to avoid numerical integrals and a closed-form expression for the correlation coefficients that is derived for the Laplacian azimuth angle distribution. A new performance metric to compare parametric and non-parametric channel models is proposed and used to show that the proposed model is a good fit to existing parametric models for low angle spreads (i.e., smaller than ten degree). A computational complexity analysis shows that the proposed method is a numerically efficient way of generating spatially correlated MIMO channels.

The work by R. W. Heath, Jr. is supported by the Office of Naval Research under grant number N00014-05-1-0169 and the National Science Foundation under grant CCF-514194. The work by D. J. Love is supported by the SBC Foundation and the National Science Foundation under grant number CCF0513916. This work has appeared in part in the IEEE Semiannual Vehicular Technology Conference, Milan, Italy, May 2004.

I. Introduction

Multiple-input multiple-output (MIMO) communication technology offers a spatial degree of freedom that can be leveraged to achieve significant capacity gains as well as improved diversity advantage [1], [2]. While the theoretical properties of MIMO communication systems have been acknowledged for some time, only now is a pragmatic perspective of MIMO communication in realistic propagation channels being developed [3]–[11]. These results show that realistic MIMO channels have significant spatial correlation due to the clustering of scatterers in the propagation environment. Unfortunately, spatial correlation generally has an adverse effect on capacity and error rate performance [3], [12]. Simulating realistic correlated channels is thus essential to predict the performance of real MIMO systems.

Spatially correlated MIMO channels are typically derived under certain assumptions about the scattering in the propagation environment. One popular correlation model, which we call the clustered channel model, assumes that groups of scatterers are modeled as clusters located around the transmit and receive antenna arrays. Clustered channel models have been validated through measurements [13], [14] and variations have been adopted in different standards such as the *IEEE 802.11n* Technical Group (TG) [15], for wireless local area networks (WLANs), and the *3GPP* Technical Specification Group (TSG) [16], for third generation cellular systems.

There are two popular approaches to simulate correlated MIMO channels based on methods derived from single-input multiple-output (SIMO) channel models (see [17] and the references therein). The first one is a *parametric* approach, which generates the MIMO channel matrix based on a geometrical description of the propagation environment (i.e., ray-tracing techniques). The second one is a *non-parametric* method, where the spatial correlation across MIMO channels is reproduced by a suitable choice of transmit and receive spatial correlation matrices. Parametric models are used to predict the performance of MIMO communication systems in realistic propagation environments, since they describe accurately the spatial characteristics of wireless links. Non-parametric models (ex. the Kronecker model [3], [8]) are defined using a reduced set of channel parameters (i.e., angle spread, mean angle of arrival/departure) and are suitable for theoretical analysis of correlated MIMO channels.

In theoretical analyses of MIMO systems, it may be desirable to study capacity and error rate performance accounting for spatial correlation effects, due to the propagation channel and the transmit/receive arrays. For this purpose, the channel spatial correlation has to be expressed in closed-form as a function of channel and array parameters. In [18], exact expressions of the spatial correlation coefficients were derived for different spatial distributions (i.e., uniform, Gaussian, Laplacian) of angles of departure/arrival for

uniform linear arrays (ULAs). This solution, however, is expressed in terms of sums of Bessel functions and does not show a direct dependence of the spatial correlation on the channel/array parameters.

In this paper, we propose new closed-form expressions of the spatial correlation matrices in clustered MIMO channels. We assume a Laplacian distribution of the angles of arrival/departure, which has been demonstrated to be a good fit for the power angular spectrum [19]–[22] and is practically used by different standards channel models [15], [16], [23]. The key insight is that a small angle approximation, which holds for moderate angle spreads (i.e., less than $\sim 10^{\text{o}}$), allows us to derive a closed-form solution for the spatial correlation function. Using our method, we can avoid the numerical integration in [18] and can easily obtain the correlation as a function of angle spread and arrivals. We develop these results for the commonly used uniform linear array (ULA) and extend these results to the uniform circular array (UCA), perhaps the next most common array geometries for future generation access points. To validate our model, we compare it against existing parametric and non-parametric channel models. To make the comparison, we propose a novel distance metric, derived from the mutual information of the MIMO channel, to evaluate the relative performance of parametric and non-parametric channel models. Then we evaluate this metric in different propagation conditions and show that, for angle spreads lower than $\sim 10^{\text{o}}$, our model is a good fit to the more realistic parametric models.

Besides the analytical tractability, another main benefit of the proposed method versus existing channel models, as we demonstrate, is a reduction in computational complexity and thus computation time required to compute the spatial correlation matrices. Because the spatial correlation matrices are a function of the cluster size and location, which are often modelled as random, system level simulations will require averaging over many correlation realizations. For example, in the context of network simulators, where many users and channels need to be simulated [24]–[31], and in detailed propagation studies of the effect of correlation [32], [33], the computational burden to simulate spatially correlated MIMO channels is a relevant issue. Our proposed channel model enables network simulations with significant computational saving, on the order of 10 to 1000 times compared to existing methods.

This paper is organized as follows. In Section II, we provide some background on the clustered MIMO channel models as well as parametric and non-parametric models. Then in Section III, we present the analytical derivation of the proposed model for ULA and UCA antenna configurations, outlining the approximation used. In Section IV, we propose a new performance metric to evaluate the relative performance of parametric and non-parametric channel models and show the performance degradation of our method due to the approximation used. Section V describes the computational complexity analysis of different channel models. Finally, in Section VI we give some remarks on the applicability of our model

in practical system simulators. Concluding remarks are given in Section VII.

II. Description of Clustered Channel Models

In this section we provide some background on clustered channel models as well as parametric and non-parametric models used in our analysis.

A. Background and Model Description

One common technique for modeling multi-path propagation in indoor environments is the Saleh-Valenzuela model [13], [34], where waves arriving from similar directions and delays are grouped into clusters. Using this method, a mean angle of arrival (AOA) or departure (AOD) is associated with each cluster and the AOAs/AODs of the sub-paths within the same cluster are assumed to be distributed according to a certain probability density function (pdf). The pdf of the AOAs/AODs is chosen to fit the empirically derived angular distribution of the AOAs/AODs, or power angular spectrum, of the channel. Note that, although the AOAs/AODs are physically distributed over the three dimensional space, it has been proven through channel measurements that most of the energy is localized over the azimuth directions [23]. Therefore, we assume the AOAs/AODs to be distributed according to a certain power azimuth spectrum (PAS). The size of a cluster is measured by the cluster angular spread (AS) defined as the standard deviation of the PAS.

A graphical representation of the clustered channel model is given in Fig. 1. Without loss of generality, we focus on modeling the receiver spatial correlation. Multiple scatterers around the receive array are modeled as clusters. We use the angle ϕ_{c} to denote the mean AOA/AOD of one cluster. Within the same cluster, each propagation path is characterized by an angle of arrival ϕ_0 and is generated according to a certain PAS. Depending on the system bandwidth, the excess delay across different paths may not be resolvable. In this case, multiple AOAs/AODs are defined with an offset ϕ_i relative to the mean AOA/AOD of the propagation path (ϕ_0). In typical channel models for indoor environments [15], the propagation paths within the same clusters are generated with the same mean AOA/AOD as the cluster and we assume $\phi_0 = \phi_{\mathrm{c}}$.

Several distributions have been proposed thus far to approximate the empirically observed PAS: the n-th power of a cosine function and uniform distributions [35]–[38], the Gaussian probability density function (pdf) [39], and the Laplacian pdf [20]–[22], [34], [40]–[42]. Through recent measurement campaigns in indoor [21], [22], [34], [41] and outdoor [19], [20], [40] environments, it has been shown that the PAS

is accurately modelled by the truncated Laplacian pdf, given by

$$P_\phi(\phi) = \begin{cases} \frac{\beta}{\sqrt{2}\sigma_\phi} \cdot \mathrm{e}^{-|\sqrt{2}\phi/\sigma_\phi|} & \text{if } \phi \in [-\pi, \pi); \\ 0 & \text{otherwise} \end{cases} \tag{1}$$

where ϕ is the random variable describing the AOA/AOD offset with respect to the mean angle ϕ_0, σ_ϕ is the standard deviation (RMS) of the PAS, and $\beta = 1/(1 - \mathrm{e}^{-\sqrt{2}\pi/\sigma_\phi})$ is the normalization factor needed to make the function integrate to one. The Laplacian pdf is also used by different standards bodies as in [15], [16], [23].

We consider a MIMO communication link with M_t transmit and M_r receive antennas. Suppose that the system is wideband and operating in an indoor environment that is accurately modelled using the clustered channel model. Under this assumption, the channel consists of multiple sample taps, which are associated with different clusters. Because the transmitted signals are bandlimited, it is sufficient to model only the discrete-time impulse response (see e.g. [43])

$$\mathbf{H}[t] = \sum_{\ell=0}^{L-1} \mathbf{H}_\ell[t]\ \delta[t - \ell] \tag{2}$$

obtained from sampling the band-limited continuous-time impulse response where t denotes the discrete-time index, L is the number of effectively nonzero channel taps (corresponding to the channel clusters), $\delta[t - \ell]$ is the Kronecker delta function[1], and $\mathbf{H}_\ell[t]$ is the $M_\mathrm{r} \times M_\mathrm{t}$ channel matrix for the ℓ-th tap. We assume that the taps are uncorrelated, thus we focus on modelling each channel tap. Hereafter, we briefly describe two common methods to generate the MIMO channel matrices $\mathbf{H}_\ell$.[2]

[1]The Kronecker delta is defined as

$$\delta[t - \ell] = \begin{cases} 1 & \text{if } t = \ell; \\ 0 & \text{otherwise.} \end{cases}$$

[2]We omit the $[t]$ notation for simplicity as normally the coherence of the channel implies that it is constant over many symbol periods.

B. Parametric Channel Model

In parametric channel models the entries of the MIMO channel matrix are expressed as a function of the channel spatial parameters. The ℓ-th matrix tap $\mathbf{H}_\ell$ is given by [44], [45][3]

$$\mathbf{H}_\ell = \frac{1}{\sqrt{N}} \sum_{i=1}^{N} \alpha_i \mathbf{a}_{\mathrm{r}}(\phi^{\mathrm{r}}_{\ell,i}) \mathbf{a}^{\dagger}_{\mathrm{t}}(\phi^{\mathrm{t}}_{\ell,i}) \tag{3}$$

where N is the number of rays per cluster, α_i is the complex Rayleigh channel coefficient, $\phi^{\mathrm{t}}_{\ell,i}$ and $\phi^{\mathrm{r}}_{\ell,i}$ are the AOD and AOA, respectively, of the i-th ray within the ℓ-th cluster, generated according to the Laplacian pdf in (1). Moreover, $\mathbf{a}_{\mathrm{t}}$ and $\mathbf{a}_{\mathrm{r}}$ are the transmit and receive array responses, respectively, given by

$$\mathbf{a}_{\mathrm{t}}(\phi^{\mathrm{t}}_{\ell,i}) = \left[1,\ \mathrm{e}^{j\Phi_1(\phi^{\mathrm{t}}_{\ell,i})},\quad \cdots\quad , \mathrm{e}^{j\Phi_{(M_{\mathrm{t}}-1)}(\phi^{\mathrm{t}}_{\ell,i})}\right]^T \tag{4}$$

$$\mathbf{a}_{\mathrm{r}}(\phi^{\mathrm{r}}_{\ell,i}) = \left[1,\ \mathrm{e}^{j\Phi_1(\phi^{\mathrm{r}}_{\ell,i})},\quad \cdots\quad , \mathrm{e}^{j\Phi_{(M_{\mathrm{r}}-1)}(\phi^{\mathrm{r}}_{\ell,i})}\right]^T \tag{5}$$

where Φ_m is the phase shift of the m-th array element with respect to the reference antenna. Note that the expression of Φ_m varies depending on the array configuration and is a function of the AOA/AOD. Equation (3) can be written in closed-form as [46](p.31)

$$\mathbf{H}_\ell = \mathbf{A}_{\mathrm{r},\ell} \mathbf{H}_\alpha \mathbf{A}^{\dagger}_{\mathrm{t},\ell} \tag{6}$$

where $\mathbf{A}_{\mathrm{t},\ell} = [\mathbf{a}_{\mathrm{t}}(\phi_{\ell,1}), ..., \mathbf{a}_{\mathrm{t}}(\phi_{\ell,N})]$, $\mathbf{A}_{\mathrm{r},\ell} = [\mathbf{a}_{\mathrm{r}}(\phi_{\ell,1}), ..., \mathbf{a}_{\mathrm{r}}(\phi_{\ell,N})]$ and $\mathbf{H}_\alpha = 1/\sqrt{N}\mathrm{diag}\,(\alpha_1, ..., \alpha_N)$. We define the channel covariance matrix for the ℓ-th tap as

$$\mathbf{R}_{H,\ell} = \mathcal{E}\left[\mathrm{vec}(\mathbf{H}_\ell)\mathrm{vec}(\mathbf{H}_\ell)^{\dagger}\right]. \tag{7}$$

C. Non-parametric Channel Model

We use the Kronecker model to describe the stochastic evolution of each matrix tap $\mathbf{H}_\ell$ as [3]

$$\mathbf{H}_\ell = \mathbf{R}^{1/2}_{\mathrm{r},\ell} \mathbf{H}_w \mathbf{R}^{T/2}_{\mathrm{t},\ell} \tag{8}$$

where $\mathbf{H}_w$ is a $M_{\mathrm{r}} \times M_{\mathrm{t}}$ matrix whose entries are independently distributed according to the complex Gaussian distribution. Moreover, $\mathbf{R}_{\mathrm{t},\ell}$ and $\mathbf{R}_{\mathrm{r},\ell}$ are the spatial correlation matrices at the transmitter and receiver, respectively, which express the correlation of the receive/transmit signals across the array

[3]We use $\mathcal{C}N(0,1)$ to denote a random variable with real and imaginary parts that are i.i.d. according to $N(0,1/2)$, * to denote conjugation, ^{T} to denote transposition, † to denote conjugation and transposition, $|\cdot|$ to denote the absolute value, $\|\cdot\|_1$ denotes the 1-norm, $\langle\cdot,\cdot\rangle$ to denote the complex vector space inner-product, $\mathrm{vec}(\cdot)$ to denote the vec-operator of matrices, and $\mathcal{E}[\cdot]$ to denote the expected value of random variables.

elements. The channel covariance matrix of the non-parametric model in (8) is given by the Kronecker product of the transmit and receive correlation matrices as

$$\mathbf{R}_{H,\ell} = \mathbf{R}_{\mathrm{t},\ell} \otimes \mathbf{R}_{\mathrm{r},\ell}. \tag{9}$$

In the clustered channel model, the coefficients of $\mathbf{R}_{\mathrm{t}}$ and $\mathbf{R}_{\mathrm{r}}$[4], for a single channel tap are characterized by a certain angular spread and angle of arrival. Since the same method is used to calculate each correlation matrix, we will use the notation $\mathbf{R}$ to refer to both the transmit or receive correlation matrix. Likewise, we will use M, instead of M_{r} or M_{t}, to indicate the number of antennas. The (m,n) entry of the matrix $\mathbf{R}$ for spaced array configurations is defined as [18], [40]

$$\mathbf{R}_{m,n} = \int_{-\pi}^{\pi} \mathrm{e}^{j[\Phi_m(\phi)-\Phi_n(\phi)]} P_\phi(\phi) \mathrm{d}\phi \tag{10}$$

where $P_\phi(\phi)$ is the Laplacian pdf in (1) and the term $\Phi_m(\phi) - \Phi_n(\phi)$ accounts for the phase difference between the m-th and n-th array element due to spacing.

III. Proposed Model of the Spatial Correlation Matrix

In this section, we derive an approximate expression of the spatial correlation matrices $\mathbf{R}$ reported in (8) for a single channel tap. We will show how to derive the closed-form of $\mathbf{R}$ under an approximation for low angle spreads for both ULA and UCA configurations.

A. Uniform Linear Array (ULA)

We express the phase shift in (10) of the m-th array element with respect to the reference antenna as a function of the AOA as

$$\Phi_m(\phi) = kdm \sin(\phi_0 - \phi) \tag{11}$$

where $m = 0, ..., M-1$, ϕ is the AOA offset with respect to the mean AOA of the cluster ϕ_0 and k is the wavenumber. Substituting (11) in (10), we express the cross-correlation coefficient of the ULA as

$$\mathbf{R}_{m,n} = \int_{-\pi}^{\pi} \mathrm{e}^{jkd(m-n)\sin(\phi_0-\phi)} \; P_\phi(\phi) \; d\phi \tag{12}$$

where $P_\phi(\phi)$ is the pdf given in (1).

Let us express the exponent of the function inside the integral as

$$\sin(\phi_0 - \phi) = \sin\phi_0 \cos\phi - \cos\phi_0 \sin\phi. \tag{13}$$

[4]We omit the subscript ℓ because we focus on a single tap.

Expanding with a first-order Taylor series (assuming $\phi \approx 0$)

$$\sin(\phi_0 - \phi) \approx \sin\phi_0 - \phi\cos\phi_0. \tag{14}$$

Substituting (14) into (12) we get

$$\mathbf{R}_{m,n} \approx \mathrm{e}^{jkd(m-n)\sin\phi_0} \cdot \int_{-\pi}^{\pi} \mathrm{e}^{-jkd(m-n)\cos(\phi_0)\phi}\, P_\phi(\phi)\, d\phi. \tag{15}$$

From (1) we observe that the truncated Laplacian PAS is zero outside the range $[-\pi, \pi)$. Therefore, the integration of $P_\phi(\phi)$ truncated over $[-\pi, \pi)$ is approximately equivalent to integration over the real line. Then, substituting (1) into (15) we get

$$[\mathbf{R}(\phi_0, \sigma_\phi)]_{m,n} \approx \mathrm{e}^{jkd(m-n)\sin\phi_0} \cdot \int_{-\infty}^{\infty} e^{-jkd(m-n)\cos(\phi_0)\phi}\, \frac{\beta}{\sqrt{2}\sigma_\phi}\mathrm{e}^{-|\sqrt{2}\phi/\sigma_\phi|}\, d\phi. \tag{16}$$

Equation (16) consists of the product of a complex exponential term times an integral term. The integral term is the characteristic function of the Laplacian pdf in (1), and it can be expressed as

$$[\mathbf{B}(\phi_0, \sigma_\phi)]_{m,n} = \int_{-\infty}^{\infty} e^{-jkd(m-n)\cos(\phi_0)\phi}\, \frac{\beta}{\sqrt{2}\sigma_\phi}\mathrm{e}^{-|\sqrt{2}\phi/\sigma_\phi|}\, d\phi = \mathcal{F}_\omega\left\{\frac{\beta}{\sqrt{2}\sigma_\phi}\mathrm{e}^{-|\sqrt{2}\phi/\sigma_\phi|}\right\} \tag{17}$$

where $\mathcal{F}_\omega$ denotes the Fourier transform evaluated at $\omega = kd(m-n)\cos\phi_0$. Solving (17), we get

$$[\mathbf{B}(\phi_0, \sigma_\phi)]_{m,n} = \frac{\beta}{1 + \frac{\sigma_\phi^2}{2} \cdot [kd(m-n)\cos\phi_0]^2} \tag{18}$$

with $m, n = 0, ..., (M-1)$. Therefore, substituting (18) in (16) we derive the following closed-form for the correlation coefficients across all the array elements

$$[\mathbf{R}(\phi_0, \sigma_\phi)]_{m,n} \approx \frac{\beta\ \mathrm{e}^{jkd(m-n)\sin\phi_0}}{1 + \frac{\sigma_\phi^2}{2} \cdot [kd(m-n)\cos\phi_0]^2}. \tag{19}$$

The complex exponential term in (16) can be written as

$$\mathrm{e}^{jkd(m-n)\sin\phi_0} = \mathrm{e}^{jkdm\sin\phi_0} \cdot \mathrm{e}^{-jkdn\sin\phi_0} \tag{20}$$

where the multiplicative factors at the right hand side of (20) are the entries of the steering vector of the ULA, given by

$$\mathbf{a}_{\mathrm{ula}}(\phi_0) = \left[1,\ \mathrm{e}^{jkd\sin\phi_0},\quad \cdots\quad, \mathrm{e}^{jkd(M-1)\sin\phi_0}\right]^T. \tag{21}$$

Using the definition in (21), we derive the spatial correlation matrix, with complex entries given by (19), as

$$\mathbf{R}(\phi_0, \sigma_\phi) \approx \left[\mathbf{a}_{\mathrm{ula}}(\phi_0) \cdot \mathbf{a}_{\mathrm{ula}}^{\dagger}(\phi_0)\right] \odot \mathbf{B}(\phi_0, \sigma_\phi) \tag{22}$$

where $\odot$ denotes the Shur-Hadamard (or elementwise) product and $\mathbf{a}(\phi_0)$ is the array response (column vector) for the mean azimuth AOA (ϕ_0). A similar result was given in [47], [48], where the Gaussian distribution was used for the PAS. In our case, however, we computed the matrix $\mathbf{R}(\phi_0, \sigma_\phi)$ for the case of Laplacian pdf, given by (1).

B. Uniform Circular Array (UCA)

We express the phase shift in (10) of the m-th array element with respect to the center of the UCA as a function of the AOA as

$$\Phi_m(\phi) = k\rho\cos\left[(\phi_0 - \phi) - \phi_m\right]. \tag{23}$$

Substituting (23) in (10) we write

$$\mathbf{R}_{m,n} = \int_{-\pi}^{\pi} \mathrm{e}^{jk\rho[\cos(\phi_0-\phi_m-\phi)-\cos(\phi_0-\phi_n-\phi)]}\; P_\phi(\phi)\; d\phi. \tag{24}$$

Consider the exponent in (24)

$$\Phi_{mn} = \cos(\phi_0 - \phi_m - \phi) - \cos(\phi_0 - \phi_n - \phi). \tag{25}$$

Applying the following trigonometric formula of angle addition

$$\cos(\alpha - \beta) = \cos\alpha\cos\beta + \sin\alpha\sin\beta \tag{26}$$

we find

$$\Phi_{mn} = [\cos(\phi_0 - \phi_m) - \cos(\phi_0 - \phi_n)]\cos\phi + [\sin(\phi_0 - \phi_m) - \sin(\phi_0 - \phi_n)]\sin\phi. \tag{27}$$

Using the first-order Taylor expansion (assuming $\phi \approx 0$)

$$\begin{aligned} \Phi_{mn} &\approx [\cos(\phi_0 - \phi_m) - \cos(\phi_0 - \phi_n)] + [\sin(\phi_0 - \phi_m) - \sin(\phi_0 - \phi_n)]\,\phi \\ &= F_{mn} + G_{mn}\phi \end{aligned} \tag{28}$$

where we defined $F_{mn} = \cos(\phi_0 - \phi_m) - \cos(\phi_0 - \phi_n)$ and $G_{mn} = \sin(\phi_0 - \phi_m) - \sin(\phi_0 - \phi_n)$. Substituting these values in (24)

$$\mathbf{R}_{m,n} \approx \mathrm{e}^{jk\rho F_{mn}} \cdot \int_{-\infty}^{\infty} \mathrm{e}^{jk\rho G_{mn}\phi}\; P_\phi(\phi)\; d\phi. \tag{29}$$

Similar to the ULA case, we identify the complex exponential term and the integral term in (29). The integral term can be expressed in terms of the characteristic function of the Laplacian pdf as

$$[\mathbf{B}(\phi_0, \sigma_\phi)]_{m,n} = \mathcal{F}_\omega\left\{\frac{1}{\sqrt{2}\sigma_\phi}\mathrm{e}^{-|\sqrt{2}\phi/\sigma_\phi|}\right\} \tag{30}$$

where $\mathcal{F}_\omega$ denotes as usual the Fourier transform evaluated at $\omega = -k\rho G_{mn}$. Then

$$[\mathbf{B}(\phi_0, \sigma_\phi)]_{m,n} = \frac{\beta}{1 + \frac{\sigma_\phi^2}{2}\cdot\left[k\rho\left(\sin(\phi_0 - m\phi_s) - \sin(\phi_0 - n\phi_s)\right)\right]^2} \tag{31}$$

where we assumed $\phi_m = m\phi_s$ and $\phi_n = n\phi_s$ for UCAs, with $m, n = 0, ..., (M-1)$. Substituting (31) in (29) and using the definition of F_{mn} given before, we can write the closed-form solution of the correlation coefficients for the UCA as

$$[\mathbf{R}(\phi_0, \sigma_\phi)]_{m,n} \approx \frac{\beta \ \mathrm{e}^{jk\rho[\cos(\phi_0 - m\phi_s) - \cos(\phi_0 - n\phi_s)]}}{1 + \frac{\sigma_\phi^2}{2} \cdot [k\rho\,(\sin(\phi_0 - m\phi_s) - \sin(\phi_0 - n\phi_s))]^2}. \tag{32}$$

The complex exponential term in (29) may be expanded as

$$\mathrm{e}^{jk\rho F_{mn}} = \mathrm{e}^{jk\rho\cos(\phi_0 - \phi_m)} \cdot \mathrm{e}^{-jk\rho\cos(\phi_0 - \phi_n)} \ . \tag{33}$$

where each complex exponential at the right hand side of (33) is the entry of the steering vector of the UCA, defined as [49]

$$\mathbf{a}_{\mathrm{uca}}(\phi_0) = \left[\mathrm{e}^{jk\rho\cos(\phi_0)},\ \mathrm{e}^{jk\rho\cos(\phi_0 - \phi_s)},\quad \cdots \quad, \mathrm{e}^{jk\rho\cos(\phi_0 - (M-1)\phi_s)}\right]^T, \tag{34}$$

where we used the usual assumption of $\phi_m = m\phi_s$ for uniformly spaced circular arrays. Finally, using (31) and the definition (34)

$$\mathbf{R}(\phi_0, \sigma_\phi) \approx \left[\mathbf{a}_{\mathrm{uca}}(\phi_0) \cdot \mathbf{a}_{\mathrm{uca}}^{\dagger}(\phi_0)\right] \odot \mathbf{B}(\phi_0, \sigma_\phi)$$

which is the same expression of the spatial correlation matrix as in (22). Note that the closed-form of $\mathbf{R}(\phi_0, \sigma_\phi)$ in (22) is the same for both the ULA and the UCA cases. The expressions of the matrix $\mathbf{B}(\phi_0, \sigma_\phi)$ and the vector $\mathbf{a}(\phi_0)$ are different, however, and they are reported respectively in (18) and (21) for the ULA case and in (31) and (34) for the UCA case.

IV. Performance Comparison of Different MIMO Channel Models

We compare the performance of the proposed non-parametric channel model against parametric models, based on metrics derived from the MIMO capacity and spatial correlation matrix. From these metrics, we evaluate the conditions under which non-parametric and parametric MIMO channel models provide the same performance. Then we determine the channel scenarios (defined by different combinations of values of ϕ_0 and σ_ϕ) for which our model provides similar performance as parametric models.

We consider three different models to generate the complex MIMO channel matrix $\mathbf{H}$:

- **Parametric model** (PM) described in (3), based on sum of N rays;
- **Exact non-parametric model** (ENPM) in (8) employing the exact correlation coefficients derived in [7] for ULAs. In [7] the closed-form expression of the spatial correlation coefficients is expressed as infinite sum of Bessel functions of the first kind. For simulation purposes, we truncate this series to a finite sum of N_{B} Bessel functions;

- **Approximate non-parametric model** (ANPM) in (8) using the approximated spatial correlation coefficients in (19) and (32) for the ULAs and UCAs, respectively.

A. Performance Metrics

To compare the relative performance of the channel models described above, we employ a well known metric defined from the channel covariance matrix [50]

$$\Psi(\mathbf{R}_1, \mathbf{R}_2) = \frac{\|\mathbf{R}_1 - \mathbf{R}_2\|_{\mathrm{F}}}{\|\mathbf{R}_1\|_{\mathrm{F}}} \tag{35}$$

where $\mathbf{R}_1$ and $\mathbf{R}_2$ are spatial correlation matrices obtained from two different models. For the PM we employ the definition of spatial correlation matrix in (7), whereas for the ENPM and ANPM we use (9).

We observe that in [51], [52] the MIMO ergodic capacity was expressed in closed-form as a function of the spatial correlation matrix. Hence, the error provided by the metric in (35) is directly related to mismatch of the ergodic capacity obtained through two different channel models. The results in [51], [52], however, are derived for non-parametric channel models employing the Kroneker structure in (8), and cannot be extended in general to parametric models in (3) (unless certain assumptions are made on the channel model [3]). Moreover, we note that the covariance matrix in (9) is parametric, whereas (7) is the average of a random matrix and its estimate may be biased. Fair comparisons of parametric versus non-parametric channel models have to rely on the distribution of the mutual information, derived from the MIMO channel matrix (rather than the spatial correlation matrices).

The mutual information of a MIMO channel, assuming equal power allocation across the transmit antennas and Gaussian signaling, is given by

$$C(\mathbf{H}) = \log_2 \left| \mathbf{I}_{M_{\mathrm{r}}} + \frac{\gamma_{\mathrm{o}}}{M_{\mathrm{t}}} \mathbf{H}\mathbf{H}^{\dagger} \right| \tag{36}$$

where γ_{o} is the average signal-to-noise ratio (SNR). From (36) it is possible to derive two metrics commonly used to evaluate the performance of MIMO systems: mean and 10% outage capacity [53]. In correlated MIMO channels, however, the Gaussian approximation [54]–[56] does not always hold (especially when the channel is high spatially correlated) and the pdf of C cannot be characterized simply by its first and second order moments. Hence, we define the following metric derived from the pdf of the mutual information in (36)

$$\begin{aligned} D_{\mathrm{pdf}}(f, g) &= \frac{\| f(C) - g(C) \|_1}{\| f(C) \|_1 + \| g(C) \|_1} \\ &= \frac{1}{2} \int_0^{\infty} | f(C) - g(C) | \, dC \end{aligned} \tag{37}$$

where $f(C)$ and $g(C)$ are the pdf's of C for different channel models, with $\| f(C) \|_1 = \| g(C) \|_1 = 1$ by definition of the pdf. Note that (37) satisfies the condition $0 \leq D_{\mathrm{pdf}}(f, g) \leq 1$, with $D_{\mathrm{pdf}}(f, g) = 0$ when $f(C) = g(C)$, $\forall C$. In the next subsection, we describe how to estimate the pdf's $f(C)$ and $g(C)$.

In the following results, we choose the PM as the reference to compare the performance of our proposed ANPM, since the PM describes more accurately the physical properties of the propagation channel and can be used to simulate any array configuration. Parametric models, however, assume a finite number of rays in the propagation environment, as opposed to non-parametric models for which the multi-paths are assumed to be continuously distributed in space. Hence, we begin by comparing the PM against the ENPM for different numbers of rays (N).

B. Performance Comparison of the PM against ENPM

Fig. 3(a) depicts the pdf of the mutual information in (36) for the PM and ENPM for ULAs, with a variable number of rays (N), $M_{\mathrm{t}} = M_{\mathrm{r}} = M = 4$, SNR$= 10$ dB, $\sigma_\phi = 50^{\mathrm{o}}$ and $\phi_0 = 0^{\mathrm{o}}$ both at transmit and receive sides. In the following results we assume the array element spacing is $d = 0.5\lambda$, with λ being the wavelength. The pdf of C is computed through Monte Carlo simulations over ten thousands channel instances and by curve fitting. Note that the Gaussian approximation can be used to fit the pdf of the MIMO channel capacity for i.i.d. and single-sided spatially correlated channels as shown in [54]–[56]. We observed, however, that the Gaussian fit becomes loose when the channel spatial correlation is high (i.e., low AS). Since our final goal is to compare the performance of ANPM against PM in any correlated scenario, we employ polynomial fitting functions to approximate the pdf of C. Fig. 3(a) shows that, as the number of rays increases from 5 to 100, the PM approaches the performance of ENPM. Similar results are given in Fig. 3(b) for the cumulative density function (CDF) of the mutual information. We observe that the PM approaches the ENPM for $N \rightarrow 100$.

Next, we compute the optimal value of N for which PM converges to ENPM, for different system parameters, by employing the metric in (37). Fig. 4 depicts the distance metric in (37) as a function of the number of rays (N) for different numbers of transmit/receive antennas $M_{\mathrm{t}} = M_{\mathrm{r}} = M$. We compare the performance of the PM with variable N against the ENPM with $N_{\mathrm{B}} = 500$. The MIMO channel is simulated with $\sigma_\phi = 50^{\mathrm{o}}$ and $\phi_0 = 0^{\mathrm{o}}$ both at transmit and receive sides. We observe that D_{pdf} decreases as N increases, since a larger number of rays for the PM more closely approximates the continuous spatial distribution of rays in the ENPM. Moreover, for fixed N, D_{pdf} increases with M due to the higher dimensionality of the MIMO channel. We empirically choose the threshold of 5% as a target value and observe that, for the practical case of $M = 4$, about 70 rays are enough for the PM to

approximate the ENPM. Note that the channel is generated with low spatial correlation (i.e., large AS), and fewer rays may be required for smaller values of σ_ϕ.

Fig. 5 depicts the metric in (35) as a function of N, for $M_{\rm t} = M$ and $M_{\rm r} = 1$ in correlated MIMO channels with $\phi_0 = 0^{\rm o}$ and variable σ_ϕ. The matrix $\mathbf{R}_1$ is generated according to the ENPM in (9), whereas the matrix $\mathbf{R}_2$ is derived from the PM in (7). We choose a target of 10% as in [50]. We observe that, for any N, the PM is a good fit to the ENPM in terms of Ψ, since single receive antenna is assumed.

C. Performance of the Proposed ANPM Against PM

Here, we compare the performance of the proposed ANPM against parametric models for ULAs and UCAs. We consider practical MIMO systems with $M_{\rm t} = M_{\rm r} = 4$ antennas and we simulate the PM with $N = 100$ rays. Moreover, we use the same channel parameters (i.e., σ_ϕ and ϕ_0) both at the transmit and receive sides. Note that we choose $N = 100$ to guarantee that the parametric model fits the non-parametric models also for large angle spread (i.e., $30^{\rm o}$). For small angle spreads and number of antennas, however, the PM fits non-parametric models also for smaller values of N as shown in Fig. 4.

Fig. 6(a) shows the metric in (36) as a function of the channel parameters for ULAs. We observe that, for values of angle spread lower than $10^{\rm o}$ and for any value of mean-AOA in the range $[0^{\rm o}, 90^{\rm o}]$, $D_{\rm pdf}$ is always below the predefined 5% target. Then, for these values of σ_ϕ and ϕ_0, the ANPM approaches the performance of PM. Similarly, Fig. 6(b) shows that the range of values for which the ANPM with UCAs approximates the PM within the 5% target of $D_{\rm pdf}$ is $\phi_0 \in [0^{\rm o}, 90^{\rm o}]$ and $\sigma_\phi \leq 5^{\rm o}$.

Fig. 7(a) and Fig. 7(b) depict the metric in (35) as a function of the channel parameters for both ULAs and UCAs. Once more, the ANPM approximates the PM within the 10% target of Ψ for any value of ϕ_0 and for σ_ϕ below $10^{\rm o}$ and $5^{\rm o}$ for the ULA and UCA, respectively. We conclude that the proposed ANPM for ULAs and UCAs is a good approximation to the PM for small angle spreads (i.e., lower than $\sim 10^{\rm o}$ for ULAs).

V. Computational Complexity Analysis

Hereafter, we analyze the computational cost of the three channel models described above and evaluate the complexity reduction of the ANPM over the PM and ENPM. In this analysis, we count the number of arithmetic functions used to compute the MIMO complex channel coefficients in (2), with $t = 1, \ldots, N_{\rm s}$ and $N_{\rm s}$ being the number of channel instances to be simulated. We assume any arithmetic function has computational cost of K, while recognizing that the value of K is machine dependent.

We first consider the case of ULA. For the PM, the cost to evaluate the ℓ-th matrix tap in (3) is $N(6N+5)(M_{\rm t}+M_{\rm r})K$. When L clusters are simulated, with $N_{\rm s}$ samples each, the total computational complexity of PM is

$$\mathcal{C}_{\rm PM} = N_{\rm s} L N(6N+5)(M_{\rm t}+M_{\rm r})K. \tag{38}$$

For the ENPM we use the approximation for Bessel functions of the first kind in [18], truncating the infinite series to the order $N_{\rm B}$. To compute numerically the Bessel functions from the order zero up to $2N_{\rm B}+1$, we employ a well known method based on polynomial approximation and backward recurrence [57]. It is possible to show that the cost to compute the complex entries of the matrices $\mathbf{R}_{{\rm t},\ell}$ and $\mathbf{R}_{{\rm r},\ell}$ in (8) for the L channel clusters is given by $\mathcal{C}_{\rm R,ENPM} = \mathcal{O}\left(62 N_{\rm B} L(M_{\rm t}^2+M_{\rm r}^2)K\right)$, for $N_{\rm B} \gg L$. Moreover, the cost for Cholesky decomposition of the transmit/receive correlation matrices is $\mathcal{C}_{\rm chol} = \mathcal{O}\left(2/3 L(M_{\rm t}^3+M_{\rm r}^3)K\right)$, and the matrix multiplication for the Kronecker model in (8) has complexity $\mathcal{C}_{\rm mult} = \mathcal{O}\left(N_{\rm s} L(6M_{\rm t}^2 M_{\rm r} + M_{\rm t} M_{\rm r}^2)K\right)$. Then, we derive the computational cost of the ENPM as

$$\mathcal{C}_{\rm ENPM} = \mathcal{C}_{\rm R,ENPM} + \mathcal{C}_{\rm chol} + \mathcal{C}_{\rm mult}. \tag{39}$$

The ANPM evaluates the transmit/receive correlation matrices through the closed-form expression in (19) with computational effort $\mathcal{C}_{\rm R,ANPM} = \mathcal{O}\left(20 L(M_{\rm t}^2+M_{\rm r}^2)K\right)$, while $\mathcal{C}_{\rm chol}$ and $\mathcal{C}_{\rm mult}$ are the same as for the ENPM. Then, the total computational complexity of ANPM is

$$\mathcal{C}_{\rm ANPM} = \mathcal{C}_{\rm R,ANPM} + \mathcal{C}_{\rm chol} + \mathcal{C}_{\rm mult}. \tag{40}$$

We now use these results to evaluate the computational saving of the ANPM over the PM and ENPM. To make our discussion concrete, we consider the case of multi-user MIMO systems with $M_{\rm t} = M$ transmit antennas and U users with $M_{\rm r} = 1$ receive antenna each. For these systems, the computational burden to generate spatial channels for all the users may be very high, especially when U is a large number. Hereafter, we demonstrate the significant complexity reduction attainable through the ANPM. From (38) and (40) we derive the computational gain of ANPM against PM as

$$G_{\rm ANPM-PM} = \frac{\mathcal{C}_{\rm PM}\cdot U}{\mathcal{C}_{\rm ANPM}\cdot U} \approx \frac{N^2}{M} \tag{41}$$

where we assumed $N \gg 1$. Equation (41) reveals that the computational gain of ANPM depends essentially on the number of rays used for the PM, given that $N \gg M$. For example, we consider the practical case of $M = 4$ and we assume $N = 70$, for which parametric models approximate non-parametric models within the 5% target of $D_{\rm pdf}$, as shown in Fig. 4. Under these assumptions, the

computational saving of ANPM over PM to calculate the MIMO channel matrix taps is $G_{\mathrm{ANPM-PM}} \approx 1200$.

Similarly, from (39) and (40), we compute the gain produced by the ANPM over the ENPM as

$$G_{\mathrm{ANPM-ENPM}} = \frac{\mathcal{C}_{\mathrm{ENPM}} \cdot U}{\mathcal{C}_{\mathrm{ANPM}} \cdot U} \approx \frac{10N_{\mathrm{B}}}{N_{\mathrm{s}}} + 1 \tag{42}$$

where we assumed $N_{\mathrm{s}} \gg M$. Assuming $N_{\mathrm{B}} = 100$ as in the IEEE 802.11n standard channel model [58] and $N_{\mathrm{s}} = 100$, we derive the computational gain of the ANPM over ENPM as $G_{\mathrm{ANPM-ENPM}} \approx 10$.

For the case of UCA, we observe that the computational complexity of the PM is the same as for ULA, since the same number of arithmetic functions is used to calculate the steering vectors in (21) and (34). Moreover, the ANPM computes the spatial correlation matrices using the proposed closed-form in (32) with computational complexity $\mathcal{C}_{\mathrm{R,ANPM}} = \mathcal{O}\left(26L(M_{\mathrm{t}}^2 + M_{\mathrm{r}}^2)K\right)$. Therefore, the gain of ANPM over PM for the UCA case is the same as in (41).

VI. Remarks on Applicability of the ANPM

We observed that the approximation for small angles employed by the ANPM limits this model to be used only for channel scenarios characterized by small angular spread (i.e., $\leq 10^{\mathrm{o}}$ for ULAs). Channel models for outdoor environments for cellular systems typically assume the AS of each tap at the base station is on the order of 5^{o}. Some examples are the 3GPP spatial channel model (SCM) [16] and the COST-259 model [23]. One practical application of the proposed ANPM is to generate spatially correlated channels for the MIMO broadcast channel with multiple transmit antennas and single receive antenna per user.

Moreover, we showed that the ANPM provides closed-form expressions of the correlation coefficients as a function of the channel parameters (i.e., angle spread, mean AOA) for ULAs and UCAs. These expressions are useful tools to analyze the performance of different arrays exploiting space diversity in clustered MIMO channel models. For example, in [59] we used the ANPM to compare the performance of space versus pattern diversity techniques in spatially correlated MIMO channels.

VII. Conclusion

We proposed closed-form expressions for generating spatial correlation matrices for clustered MIMO channel models. Our approach assumes a Laplacian power azimuth spectrum and uses a small angle approximation to obtain a closed-form solution for the spatial correlation matrix that is valid for either uniform linear arrays or circular arrays. Despite its simple analytical tractability, the proposed method

fits more complex (but more exact) methods proposed in the literature for angle spreads less than 10^o, thereby reducing the computational complexity to simulate correlated MIMO channels. The proposed method is a computationally efficient solution for network simulators, where spatially correlated MIMO channels have to be simulated for a large number of users.

REFERENCES

[1] D. Gesbert, M. Shafi, D.-S. Shiu, P. J. Smith, and A. Naguib, "From theory to practice: an overview of MIMO space-time coded wireless systems," *IEEE Jour. Select. Areas in Comm.*, vol. 21, no. 3, pp. 681–683, June 2003.

[2] A. Goldsmith, S. A. Jafar, N. Jindal, and S. Vishwanath, "Capacity limits of MIMO channels," *IEEE Jour. Select. Areas in Comm.*, vol. 21, no. 5, pp. 684–702, June 2003.

[3] D.-S. Shiu, G. J. Foschini, M. J. Gans, and J. M. Kahn, "Fading correlation and its effect on the capacity of multielement antenna systems," *IEEE Trans. Comm.*, vol. 48, no. 3, pp. 502–513, Mar. 2000.

[4] D. Chizhik, F. Rashid-Farrokhi, J. Ling, and A. Lozano, "Effect of antenna separation on the capacity of BLAST in correlated channels," *IEEE Comm. Lett.*, vol. 4, pp. 337–339, Nov. 2000.

[5] J. Fuhl, A. F. Molisch, and E. Bonek, "Unified channel model for mobile radio systems with smart antennas," *IEE Proceedings on Radar, Sonar and Navigation*, vol. 145, pp. 32 – 41, Feb. 1998.

[6] J. W. Wallace and M. A. Jensen, "Modeling the indoor MIMO wireless channel," *IEEE Trans. Antennas Propagat.*, vol. 50, no. 5, pp. 591–599, May 2002.

[7] J. P. Kermoal, L. Schumacher, P. E. Mogensen, and K. I. Pedersen, "Experimental investigation of correlation properties of MIMO radio channels for indoor picocell scenarios," vol. 1, pp. 14–21, Sep. 2000.

[8] J. P. Kermoal, L. Schumacher, K. I. Pedersen, P. E. Mogensen, and F. Frederiksen, "A stochastic MIMO radio channel model with experimental validation," *IEEE Jour. Select. Areas in Comm.*, vol. 20, no. 6, pp. 1211–1226, Aug. 2002.

[9] C. Oestges, V. Erceg, and A. J. Paulraj, "A physical scattering model for MIMO macrocellular broadband wireless channels," *IEEE Jour. Select. Areas in Comm.*, vol. 21, no. 5, pp. 721–729, June 2003.

[10] D. S. Baum, D. Gore, R. Nabar, S. Panchanathan, K.V.S. Hari, V. Erceg, and A. J. Paulraj, "Measurement and characterization of broadband MIMO fixed wireless channels at 2.5 GHz," *Proc. IEEE Conf. on Pers. Wireless Comm.*, pp. 203–206, Dec. 2000.

[11] A. F. Molisch, "A generic model for MIMO wireless propagation channels in macro- and microcells," *IEEE Trans. Sig. Proc.*, vol. 52, pp. 61 – 71, Jan. 2004.

[12] D. Gore, R. Heath, and A. Paulraj, "Statistical antenna selection for spatial multiplexing systems," *Proc. IEEE Int. Conf. on Comm.*, vol. 1, pp. 450–454, Apr. 2002.

[13] A. A. M. Saleh and R. A. Valenzuela, "A statistical model for indoor multipath propagation," *IEEE Jour. Select. Areas in Comm.*, vol. SAC-5, no. 2, pp. 128–137, Feb. 1987.

[14] J. W. Wallace and M. A. Jensen, "Statistical characteristics of measured MIMO wireless channel data and comparison to conventional models," *Proc. IEEE Veh. Technol. Conf.*, vol. 2, no. 7-11, pp. 1078–1082, Oct. 2001.

[15] V. Erceg et al., "TGn channel models," *IEEE 802.11-03/940r4*, May 2004.

[16] 3GPP Technical Specification Group, "Spatial channel model, SCM-134 text V6.0," *Spatial Channel Model AHG (Combined ad-hoc from 3GPP and 3GPP2)*, Apr. 2003.

[17] R. B. Ertel, P. Carderi, K. W. Sowerby, T. S. Rappaport, and J. H. Reed, "Overview of spatial channel models for antenna array communication systems," *Proc. IEEE Conf. on Pers. Wireless Comm.*, pp. 10–22, Feb. 1998.

[18] L. Schumacher, K. I. Pedersen, and P.E. Mogensen, "From antenna spacings to theoretical capacities - guidelines for simulating MIMO systems," *Proc. IEEE Int. Symp. on Pers., Indoor and Mobile Radio Comm.*, vol. 2, pp. 587–592, Sep. 2002.

[19] K. I. Pedersen, P. E. Mogensen, and B. H. Fleury, "Power azimuth spectrum in outdoor environments," *Electronics Letters*, vol. 33, no. 18, pp. 1583–1584, Aug. 1997.

[20] K. I. Pedersen, P. E. Mogensen, and B. H. Fleury, "A stochastic model of the temporal and azimuthal dispersion seen at the base station in outdoor propagation environments," *IEEE Trans. on Veh. Technol.*, vol. 49, no. 2, pp. 437–447, Mar. 2000.

[21] Q. H. Spencer, B. D. Jeffs, M. A. Jensen, and A. Lee Swindlehurst, "Modeling the statistical time and angle of arrival characteristics of an indoor multipath channel," *IEEE Jour. Select. Areas in Comm.*, vol. 18, no. 3, pp. 347–360, Mar. 2000.

[22] G. German, Q. Spencer, L. Swindlehust, and R. Valenzuela, "Wireless indoor channel modeling: statistical agreement of ray tracing simulations and channel sounding measurements," *Proc. IEEE Int. Conf. Acoust., Speech and Sig. Proc.*, vol. 4, pp. 2501–2504, May 2001.

[23] L. M. Correia, *Wireless Flexible Personalised Communications*, John Wiley and Sons, Inc., New York, NY, USA, 2001.

[24] J. Wigard and P. Mogensen, "A simple mapping from C/I to FER and BER for a GSM type of air-interface," *Proc. IEEE Int. Symp. on Pers., Indoor and Mobile Radio Comm.*, vol. 1, pp. 78 – 82, Oct. 1996.

[25] H. Olofsson, M. Almgren, C. Johansson, M. Hook, and F. Kronestedt, "Improved interface between link level and system level simulations applied to GSM," *IEEE 6th International Conference on Universal Personal Communications Record*, vol. 1, pp. 79 – 83, Oct. 1997.

[26] J. Wigard, T. T. Nielsen, P. H. Michaelsen, and P. Mogensen, "BER and FER prediction of control and traffic channels for a GSM type of air-interface," *Proc. IEEE Veh. Technol. Conf.*, vol. 2, pp. 1588 – 1592, May 1998.

[27] C. Caini and G. Riva, "A new vector quantization technique for performance evaluation in frequency hopping mobile radio systems," *IEEE Comm. Lett.*, vol. 2, pp. 252 – 254, Aug. 2000.

[28] R. J. Punnoose, P. V. Nikitin, and D. D. Stancil, "Efficient simulation of Ricean fading within a packet simulator," *Proc. IEEE Veh. Technol. Conf.*, vol. 2, pp. 764 – 767, Sep. 2000.

[29] D. J. Mazzarese and W. A. Krzymien, "High throughput downlink cellular packet data access with multiple antennas and multiuser diversity," *Proc. IEEE Veh. Technol. Conf.*, vol. 2, pp. 1079 – 1083, Apr. 2003.

[30] M. Pukkila, G. P. Mattellini, and P. A. Ranta, "Constant modulus single antenna interference cancellation for GSM," *Proc. IEEE Veh. Technol. Conf.*, vol. 1, pp. 584–588, May 2004.

[31] P. A. Ranta, H. Berg, E. Tuomaala, and Z. Uykan, "Dual antenna diversity reception for EGPRS terminals," *Proc. IEEE Veh. Technol. Conf.*, vol. 1, pp. 510–514, May 2004.

[32] M. Dohler, J. Dominguez, and H. Aghvami, "Link capacity analysis for virtual antenna arrays," *Proc. IEEE Veh. Technol. Conf.*, vol. 1, pp. 440 – 443, Sep. 2002.

[33] A. Kastrisios, M. Dohler, and H. Aghvami, "Influence of channel characteristics on the performance of VAA with deployed STBCs," *Proc. IEEE Veh. Technol. Conf.*, vol. 2, pp. 1138 – 1142, Apr. 2003.

[34] Q. Spencer, M. Rice, B. Jeffs, and M. Jensen, "A statistical model for angle of arrival in indoor multipath propagation," *Proc. IEEE Veh. Technol. Conf.*, vol. 3, pp. 1415–1419, May 1997.

[35] W.C.Y. Lee, "Effects on the correlation between two mobile radio base-station antennas," *IEEE Trans. Comm.*, vol. COM-21, no. 11, pp. 1214–1224, Nov. 1973.

[36] W. Lee, "Effects on correlation between two mobile radio base-station antennas," *IEEE Trans. Comm.*, vol. 21, no. 11, pp. 1214 – 1224, Nov. 1973.

[37] W. C. Jakes, *Microwave Mobile Communications*, IEEE Press, 445 Hoes Lane, P.O. Box 1331, Piscataway, New Jersey 08855-1331, 1974.

[38] J. Salz and J. H. Winters, "Effect of fading correlation on adaptive arrays in digital mobile radio," *IEEE Trans. on Veh. Technol.*, vol. 43, no. 4, pp. 1049–1057, Nov. 1994.

[39] M. T. Feeney and J. D. Parsons, "Cross-correlation between 900 MHz signal received on vertically separated antennas in small-cell radio systems," *IEE Proceedings I*, vol. 138, no. 2, pp. 81–86, Apr. 1991.

[40] K. I. Pedersen, P. E. Mogensen, and B. H. Fleury, "Spatial channel characteristics in outdoor environments and their impact on BS antenna system performance," *Proc. IEEE Veh. Technol. Conf.*, vol. 2, pp. 719–723, 1998.

[41] A. S. Y. Poon and M. Ho, "Indoor multiple-antenna channel characterization from 2 to 8 GHz," *Proc. IEEE Int. Conf. on Comm.*, vol. 5, pp. 3519–3523, May 2003.

[42] R. J. Cramer, R. A. Scholtz, and M. Z. Win, "Evaluation of an Ultra-Wide-Band propagation channel," *IEEE Trans. Antennas Propagat.*, vol. 50, no. 5, pp. 561–570, May 2002.

[43] H. Bölcskei, M. Borgmann, and A. J. Paulraj, "Impact of the propagation environment on the performance of space-frequency coded MIMO-OFDM," *IEEE JSAC*, vol. 21, pp. 427 – 439, Apr. 2003.

[44] M. Stege, J. Jelitto, M. Bronzel, and G. Fettweis, "A multiple input-multiple output channel model for simulation of Tx- and Rx-diversity wireless systems," *Proc. IEEE Veh. Technol. Conf.*, vol. 2, pp. 833–839, Sep. 2000.

[45] A. F. Molisch, "A generic model for MIMO wireless propagation channels in macro- and microcells," *IEEE Trans. Sig. Proc.*, vol. 52, pp. 61–71, Jan. 2004.

[46] K. Yu, *Multiple-Input Multiple-Output Radio Propagation Channels: Characteristics and Models*, Doctoral Thesis, KTH Signal Sensor and Systems, Stockholm, Sweden, 2005.

[47] B. Ottersten, "Spatial division multiple access (SDMA) in wireless communications," *Signal Processing, in Proc. of Nordic Radio Symposium*, 1995.

[48] B. Ottersten, "Array processing for wireless communications," *8th IEEE Signal Processing Workshop on Statistical Signal and Array Processing*, Mar. 1996.

[49] A. Forenza and R. W. Heath Jr., "Impact of antenna geometry on MIMO communication in indoor clustered channels," *Proc. IEEE Antennas and Prop. Symp.*, vol. 2, pp. 1700 – 1703, June 2004.

[50] Kai Yu, M. Bengtsson, B. Ottersten, D. McNamara, P. Karlsson, and M. Beach, "Modeling of wide-band MIMO radio channels based on NLOS indoor measurements," *IEEE Trans. on Veh. Technol.*, vol. 53, pp. 655– 665, May 2004.

[51] M. Kiessling and J. Speidel, "Mutual information of MIMO channels in correlated Rayleigh fading environments - a general solution," *Proc. IEEE Int. Conf. on Comm.*, vol. 2, pp. 814 – 818, Jun. 2004.

[52] A. Forenza, M. R. McKay, A. Pandharipande, R. W. Heath Jr., and I. B. Collings, "Adaptive MIMO transmission for exploiting the capacity of spatially correlated channels," *submitted to IEEE Trans. on Veh. Technol.*, May 2005.

[53] A. Paulraj, R. Nabar, and D. Gore, *Introduction to Space-Time Wireless Communications*, Cambridge University Press, 40 West 20th Street, New York, NY, USA, 2003.

[54] P. J. Smith and M. Shafi, "On a gaussian approximation to the capacity of wireless MIMO systems," *Proc. IEEE Int. Conf. on Comm.*, vol. 1, pp. 406 – 410, Apr. 2002.

[55] P. J. Smith, S. Roy, and M. Shafi, "Capacity of MIMO systems with semicorrelated flat fading," *IEEE Trans. Info. Th.*, vol. 49, pp. 2781 – 2788, Oct. 2003.

[56] P. J. Smith and M. Shafi, "An approximate capacity distribution for MIMO systems," *IEEE Trans. Comm.*, vol. 52, pp. 887 – 890, June 2004.

[57] S. Zhang and J. Jin, *Computation of Special Functions*, John Wiley and Sons, Inc., 605 Third Avenue, New York, NY, 10158-0012, 1996.

[58] L. Schumacher, "WLAN MIMO channel Matlab program," download information: http:\\www.info.fundp.ac.be\ ∼lsc\Research\IEEE_80211_HTSG_CMSC\distribution_terms.html.

[59] A. Forenza and R. W. Heath Jr., "Benefit of pattern diversity via 2-element array of circular patch antennas in indoor clustered MIMO channels," *IEEE Trans. Comm.*, vol. 54, pp. 943–954, May 2006.

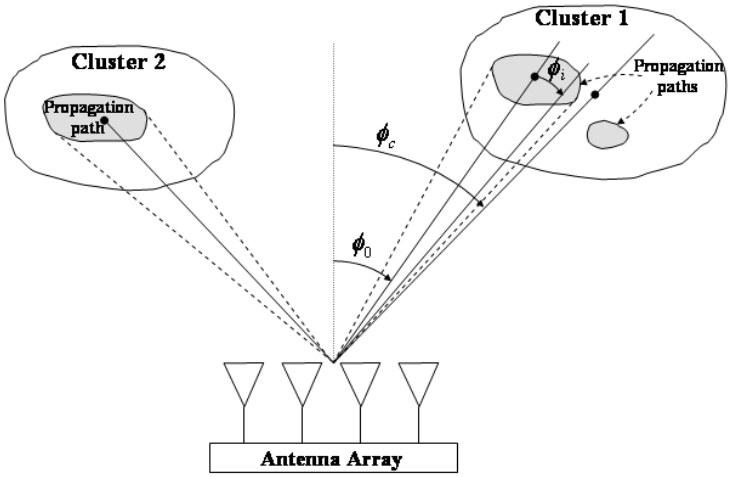

Fig. 1. Geometry of the model representing clusters and propagation paths. The angles ϕ_c and ϕ_0 are the mean AOAs of the cluster and propagation paths, respectively. The angle ϕ_i is the AOA offset of the path.

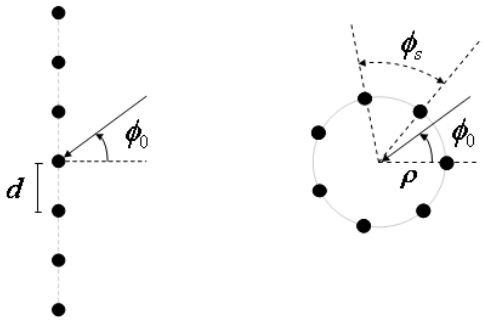

Fig. 2. Uniform linear array (ULA) and uniform circular array (UCA) configurations, 7-element case.

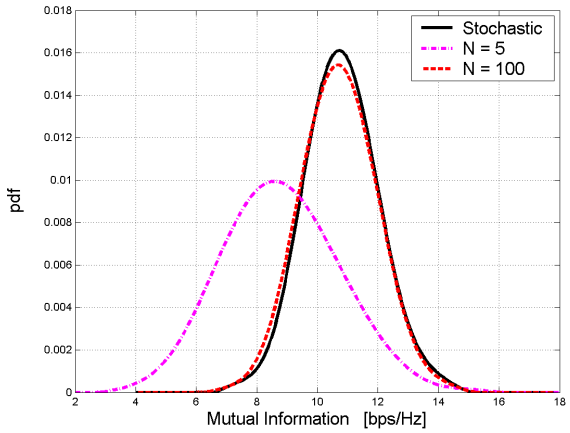

(a) pdf

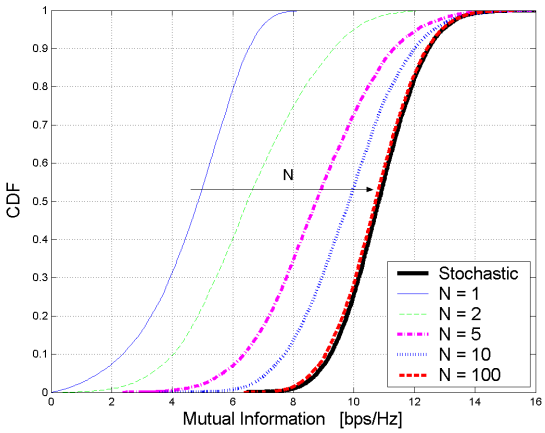

(b) CDF

Fig. 3. Probability density function (pdf) and cumulative density function (CDF) of the mutual information for PM and ENPM with variable number of rays (N). The same number of transmit/receive antennas (i.e., $M_{\mathrm{t}} = M_{\mathrm{r}} = 4$) and single cluster channel with $\sigma_\phi = 50^{\mathrm{o}}$ and $\phi_0 = 0^{\mathrm{o}}$ were used.

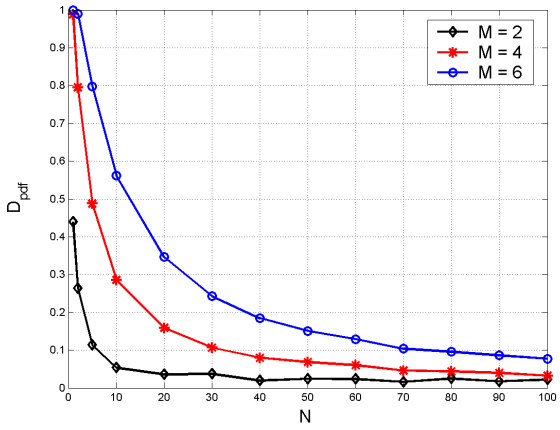

Fig. 4. Distance between the pdf of C as a function of the number of rays, for PM and ENPM. The same number of transmit/receive antennas (i.e., $M_{\mathrm{t}} = M_{\mathrm{r}} = M$) and single cluster channel with AS $\sigma_\phi = 50^{\mathrm{o}}$ and $\phi_0 = 0^{\mathrm{o}}$ were used.

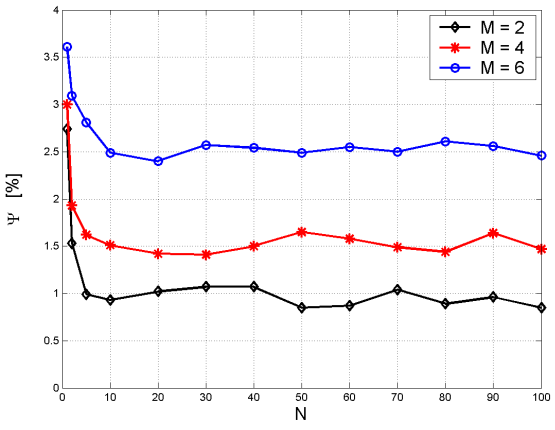

Fig. 5. Distance Ψ between the spatial correlation matrices for PM and ENPM. ULA is assumed with $M_{\mathrm{t}} = 4$, $M_{\mathrm{r}} = 1$. The channel is simulated with $\phi_0 = 0^{\mathrm{o}}$ and different values of σ_ϕ.

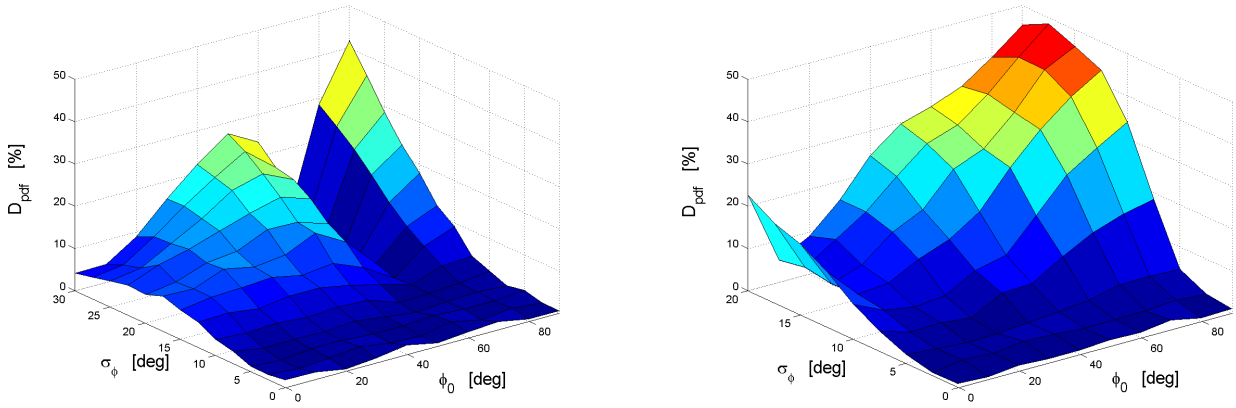

(a) ULA (b) UCA

Fig. 6. Distance between the pdf of C as a function of AS and mean-AOA, for PM and ANPM. The same number of transmit/receive antennas (i.e., $M_{\mathrm{t}} = M_{\mathrm{r}} = M = 4$) is assumed with ULA and UCA.

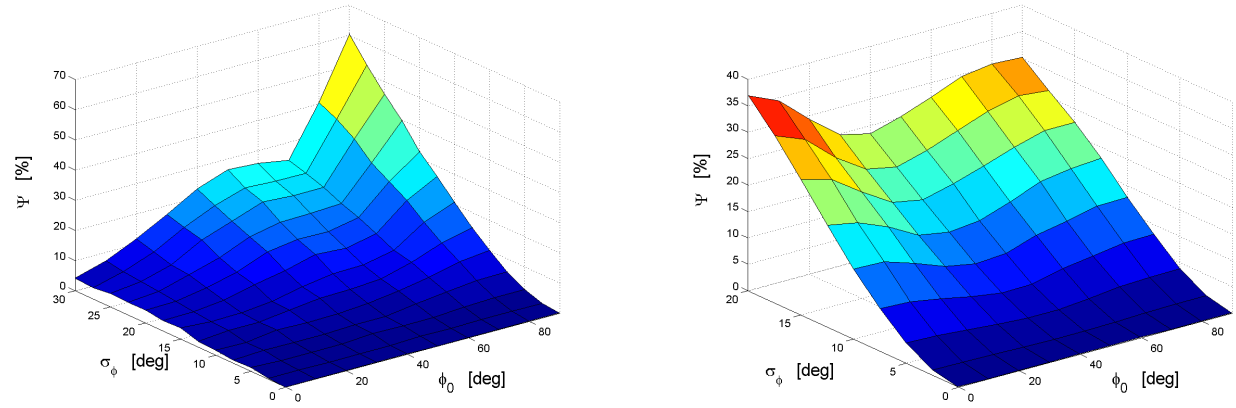

(a) ULA (b) UCA

Fig. 7. Distance Ψ between the spatial correlation matrices for PM and ANPM. The same number of transmit/receive antennas (i.e., $M_{\mathrm{t}} = M_{\mathrm{r}} = M = 4$) with ULA and UCA.